Tunable ultra-wideband terahertz filter based on three-dimensional arrays of H-shaped plasmonic crystals*

Yuan Cai(袁 偲), Xu Shi-Lin(徐世林)†, Yao Jian-Quan(姚建铨),
Zhao Xiao-Lei(赵晓蕾), Cao Xiao-Long(曹小龙), and Wu Liang(吴 亮)

Institute of Laser and Opto-electronics, Key Laboratory of Optoelectronic Information Science and Technology, College of Precision Instrument and Opto-electronics Engineering, Tianjin University, Tianjin 300072, *China*

(Received 25 April 2013; revised manuscript received 8 August 2013; published 3 December 2013)

A face-to-face system of double-layer three-dimensional arrays of H-shaped plasmonic crystals is proposed, and its transmission and filtering properties are investigated in the terahertz regime. Simulation results show that our design has excellent filtering properties. It has an ultra-wide bandgap and passband with steep band-edges, and the transmittance of the passband and the forbidden band are very close to 1 and 0, respectively. As the distance between the two face-to-face plates increases, the resonance frequency exhibits a gradual blueshift from 0.88 THz to 1.30 THz. Therefore, we can dynamically control the bandwidths of bandgap and passband by adding a piezoelectric ceramic plate between the two crystal plates. Furthermore, the dispersion relations of modes and electric field distributions are presented to analyze the generation mechanisms of bandgaps and to explain the location of bandgaps and the frequency shift phenomenon. Due to the fact that our design can provide many resonant modes, the bandwidth of the bandgaps can be greatly broadened. This paper can serve as a valuable reference for the design of terahertz functional devices and three-dimensional terahertz metamaterials.

Keywords: terahertz, wideband filter, plasmonic crystal, metamaterials

PACS: 81.05.Xj, 42.25.Bs, 78.20.–e, 46.40.Ef **DOI:** 10.1088/1674-1056/23/1/018102

1. Introduction

Terahertz (THz) radiation has broad applications in many fields—THz sensing, imaging, spectroscopy, communication, and so on.[1–4] However, due to the scarcity of THz functional devices that can be used to control and manipulate THz waves, practical technology in the THz range is still far less developed than that in other frequency ranges. It was recently shown that this limitation can be overcome by the use of metamaterials.[5–9] Many intriguing phenomena based on metamaterials have been studied intensively,[10] such as negative index of refraction,[11] diffraction-limit breaking imaging,[12] and cloaking.[13] THz metamaterials are a new class of artificial electromagnetic materials which consist of periodically arranged subwavelength units which work at THz frequencies. Among these THz metamaterials, photonic bandgap devices, especially plasmonic crystal devices, have been confirmed to be an effective means to manipulate THz waves.[14,15]

Recently, periodically structured plasmonic crystal films embedded in a metallic parallel-plate waveguide (PPWG) have attracted much attention because of specific electromagnetic properties and strong confinement of THz waves.[16–19] The bandgaps of plasmonic crystals, which resemble the photonic bandgaps of photonic crystals, are actually Bragg reflection bands. Plasmonic crystal structure is mainly made of metal, which shows high transmittance and has very steep rising and falling edges. Therefore, a plasmonic crystal structure is excellent for filtering THz waves.

Conventional single-layer plasmonic crystal films etched on the surface of PPWG have many defects. For example, the resonance strength is insufficient; filtering and modulation depth is also inadequate; and the filter bandwidth (resonance frequency range) is relatively narrow (~ 0.1 THz).[18] At present, the properties of plasmonics have been studied extensively in the optical regime,[20–25] and most of the studies are based on Bragg grating structures[24] or a one-dimensional T shaped groove.[21–23] However, the transmission performance and electromagnetic properties of three-dimensional (3D) plasmonic crystal in the THz range are still poorly understood, and to our knowledge, a double-layer system of face-to-face 3D plasmonic crystals has never been proposed before.

In this paper, we first present a system of face-to-face 3D arrays of H-shaped plasmonic crystals and numerically simulate its characteristics in the THz regime by employing the 3D finite difference time-domain (FDTD) method. The simulation results show that the 3D plasmonic crystal exhibits excellent ultra-wideband THz filtering characteristics. The relationship between the structural parameters and the filtering properties has also been investigated. The design yields an ultra-wideband blueshift from 0.88 THz to 1.30 THz as the distance between the two plates is increased. If a piezoelectric ceramic

*Project supported by the National Natural Science Foundation of China (Grant Nos. 61271066, 61101058, and 61107086) and the Science and Technology Committee of Tianjin Province, China (Grant No. 11JCYBJC01100).

†Corresponding author. E-mail: xushilin80@163.com

© 2014 Chinese Physical Society and IOP Publishing Ltd

plate is embedded between the two crystal plates, tunability of the bandgap, and the passband can be achieved easily. We also find that the resonant frequency has a significant redshift with the change of the groove depth. In addition, according to the dispersion relation, we provide the band structure of our 3D plasmonic crystal, and also offer a reasonable explanation for the frequency shift phenomenon. Lastly, for an intuitive understanding of the resonance, the electric field distributions are presented succinctly.

2. Structures and material properties

In this review, aluminum films are assumed to form the 3D inverted H-shaped plasmonic crystal. In the THz regime, aluminum has low loss and high reflectivity, similar to the ideal conductor. The permittivity of aluminum can be described by the Drude model[26]

$$\varepsilon(\omega)=\varepsilon_{\infty}-\frac{\omega_{\mathrm{p}}^2}{\omega^2+\mathrm{i}\omega/\tau}, \tag{1}$$

where ω is the angular frequency of incident THz, τ is the relaxation time of free carriers, and ε_{∞} is a constant that represents the high-frequency limit of permittivity.

Surface plasmon polaritons (SPPs) are electromagnetic excitations propagating along the interface between dielectrics and metals. Their electromagnetic fields are evanescently confined in the perpendicular direction and decay exponentially away from the planar interface.[27] In terms of an ideal metal, whose electron system behaves as a free-electron gas, SPPs arise via the coupling of the electromagnetic fields to the oscillations of the conductor's electron plasma. The dispersion of the SPPs mode can be described by

$$\beta=k_0\left[\frac{\varepsilon_{\mathrm{d}}\left(1-\omega_{\mathrm{p}}^2/\omega^2\right)}{\varepsilon_{\mathrm{d}}+\left(1-\omega_{\mathrm{p}}^2/\omega^2\right)}\right]^{1/2}, \tag{2}$$

where β is the wave vector of the SPPs, ω and k_0 are the frequency and wave vector of the incident light, and ε_{d} is the permittivity of the dielectric. By Eq. (2), the dispersion of the SPPs will follow the light line only near the long wavelength limit $\omega \ll \omega_{\mathrm{p}}$, the dispersion of the SPPs will follow the light line. Otherwise, a mismatch between the surface plasmon wave vector and the wave vector of incident light always exists.

A periodic structure, such as a sinusoidal grating, on a surface can scatter incident light through Bragg reflections.[28] In fact, the 3D double-layer oppositely arranged inverted H-shaped plasmonic crystal we designed could be treated as a 3D Bragg grating. This scattering elongates the region in momentum space which enables the incident light to couple with the conductor's electron plasma. The periodic structure with a period λ_{g} could offer an additional wavenumber k_{g}, so the scattering can compensate additional momentum to the incident light.[29]

Figure 1 shows a schematic view and geometric parameters of the 3D double-layer plasmonic crystal system, which is composed of two monolayers arranged face-to-face. Figure 1(a) is a perspective view of a single-layer plasmonic crystal. The monolayer plasmonic crystal can be considered to have two sections: the lower metal plate layer and the upper periodic structure, H is the height of the periodic structure (groove depth) and L is the distance between the two plasmonic crystal plates. We assume THz waves propagate along the gap between the two plates, and the direction of polarization of the incident THz electric field is perpendicular to the two plates, $\boldsymbol{E}$, $\boldsymbol{H}$, and $\boldsymbol{k}$ (in Fig. 1(c)) represent electric field, magnetic field, and wave vector, respectively.

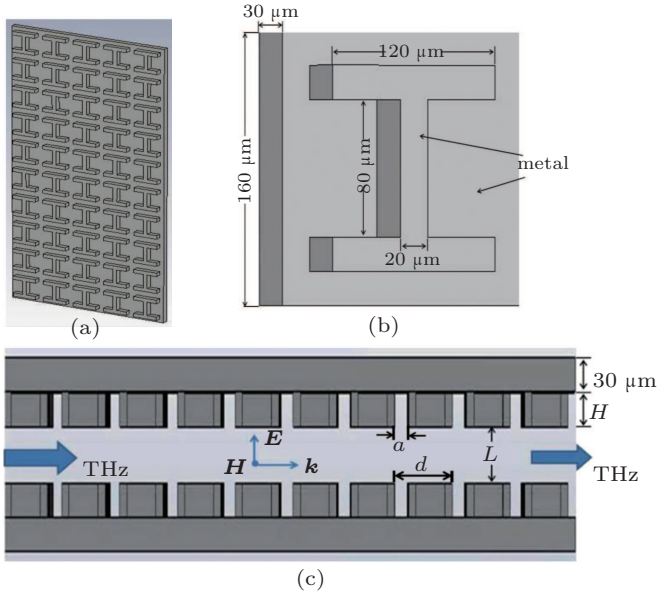


Fig. 1. (color online) Schematic view and geometric parameters of the double-layer system of 3D H-shaped plasmonic crystal arrays on plasmonic crystal film inside a metallic parallel-plate waveguide. (a) Schematic view of a single layer. (b) The geometric structure of unit cell. (c) Lateral view of the 3D double-layer plasmonic crystal system, which is composed of two oppositely arranged single-layer plasmonic crystals.

3. Theoretical calculation and analysis

The transmission spectra with various distances L from 20 μm to 100 μm and a fixed height $H = 30$ μm are simulated using the FDTD method, as shown in Fig. 2. It can be learned from Fig. 2 that our design has excellent filtering characteristics: the passband and bandgap are both ultra-wide; the transmittance of the passband and the forbidden band are very close to 1 and 0, respectively; and the band-edge is very steep. As can be seen from Fig. 2, when the distance is relatively small ($L \leq 60$ μm), the bandwidth of the bandgap is more than 2 THz; however, as the distance increases, the first cut-off frequency blueshifts gradually from 0.88 THz to 1.30 THz. Consequently, the bandwidth of the bandgap will be significantly

reduced and the bandwidth of the passband at low frequency will increase correspondingly. If a piezoelectric ceramic plate with a high piezoelectric coefficient is added between the two crystal plates, the distance L can be tuned by applied electric field. Through this method, we can dynamically control the bandwidths of bandgap and passband, and dynamically regulate the ratio between the passband and bandgap. Therefore, our design can be used as a tunable filter, and in fact, it can also be used as a voltage-controlled THz switch, operating at 0.88–1.30 THz, that can achieve a transition of transmittance almost from 0 to 1 (corresponding to off-state and on-state, respectively).

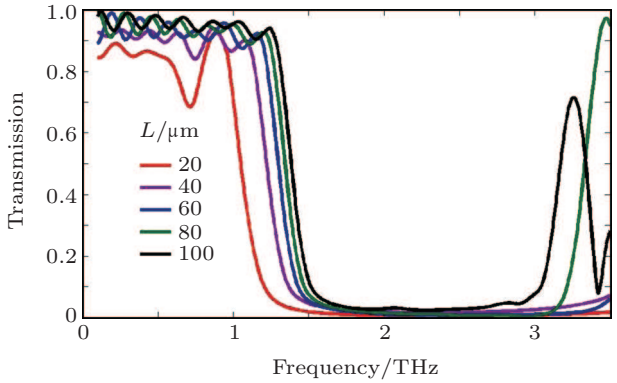


Fig. 2. Simulated transmission spectra of the 3D plasmonic crystal with different distances L between the two plates. The groove depth is constant, at $H = 30$ μm.

Plasmonic crystals also have a bandgap structure similar to that of photonic crystals. The electromagnetic waves in the bandgaps have strong resonances. Since our 3D plasmonic crystal structure can be regarded as a 3D Bragg grating, the dispersion relation of the transverse magnetic (TM) mode is described by[30]

$$1 = \frac{k_0}{\sqrt{\beta^2 - k_0^2}} \frac{a}{d} \tan(k_0 H) \times \left[\frac{(\sqrt{\beta^2 - k_0^2})/k_0 - (a/d)\tanh(L\sqrt{\beta^2 - k_0^2})\tan(k_0 H)}{(\sqrt{\beta^2 - k_0^2})/k_0 \tanh(L\sqrt{\beta^2 - k_0^2}) - (a/d)\tan(k_0 H)} \right], \quad (3)$$

where β is the mode propagation constant, k_0 is the free space wave vector, and a, d, H, and L are the geometric parameters shown in Fig. 1.

In accordance with Eq. (3), we obtain the dispersion diagram of our 3D double-layer plasmonic crystal with distance $L = 20$ μm and height $H = 30$ μm, as shown in Fig. 3(a). In Fig. 3(b), we plot its transmission spectrum on a logarithmic scale. It can be seen from Fig. 3(b) that our 3D double-layer plasmonic crystal contains two resonant modes, the center frequencies of which are 1.52 THz and 2.90 THz, respectively. This is consistent with the bandgaps shown in Fig. 3(a).

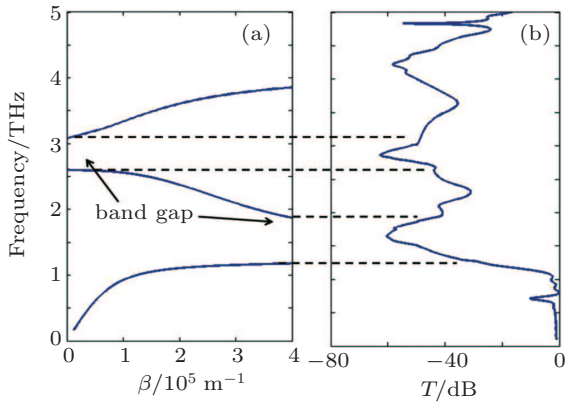


Fig. 3. (a) Dispersion diagram of the 3D double-layer inverted H-shaped plasmonic crystal, calculated according to Eq. (3), with the distance $L = 20$ μm and the groove depth $H = 30$ μm. (b) The corresponding transmission spectrum (dB), when $L = 20$ μm and $H = 30$ μm.

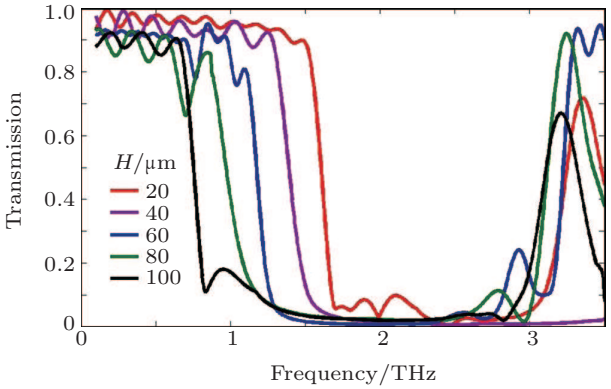


Fig. 4. Simulated transmission spectra of the 3D plasmonic crystal with various groove depths H and fixed distance $L = 60$ μm.

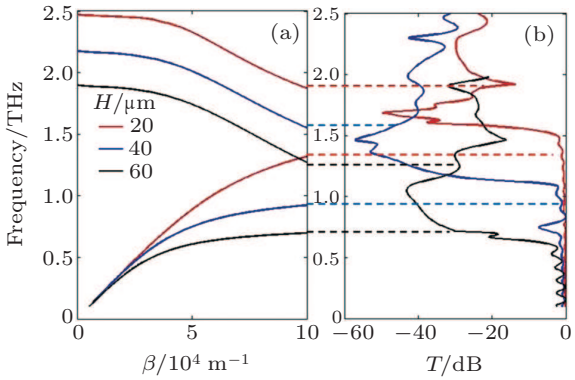


Fig. 5. (a) Dispersion diagram of our 3D double-layer plasmonic crystal with different groove depths H and fixed distance $L = 60$ μm. (b) The corresponding transmission spectra (dB).

Next, we study the influence of groove depth H on filtering characteristics of the 3D plasmonic crystal, and figure 4 shows the transmission spectra with various H with distance $L = 60$ μm unchanged. A phenomenon to be noted in Fig. 4 is that the cut-off resonance frequency moves to lower frequencies with increased groove depth H: the cut-off frequency is 1.51 THz for $H = 20$ μm and 0.64 THz for $H = 60$ μm. We can also learn from Fig. 4 that a height H of the plasmonic crystal that is either too large or too small will affect the resonances adversely, especially high frequency ones, because there are

many irregularly guided modes in the high frequency range, which show up in a spectrum as protrusions. However, when the groove depth is moderate (for example, $H = 30$ μm), there will be few protrusions at high frequency and the bandwidth of the bandgap is the biggest. This indicates that an optimal coupling height that would bring about the strongest resonance may exist.

Figure 5(a) is the dispersion diagram of the 3D double-layer plasmonic crystal with different groove depths H and fixed distance $L = 60$ μm, and figure 5(b) is its transmission spectra on a logarithmic scale. From Fig. 5(a), we can find that as H increases, the first order bandgap redshifts gradually. (When H increases from 20 μm to 60 μm, the frequency range of the first order bandgap gradually shifts from 1.41–1.90 THz to 0.74–1.26 THz.) The dispersion curves in Fig. 5(a) are basically consistent with the right transmission spectra in Fig. 5(b), and they provide a reasonable explanation for the redshift phenomenon in Fig. 4.

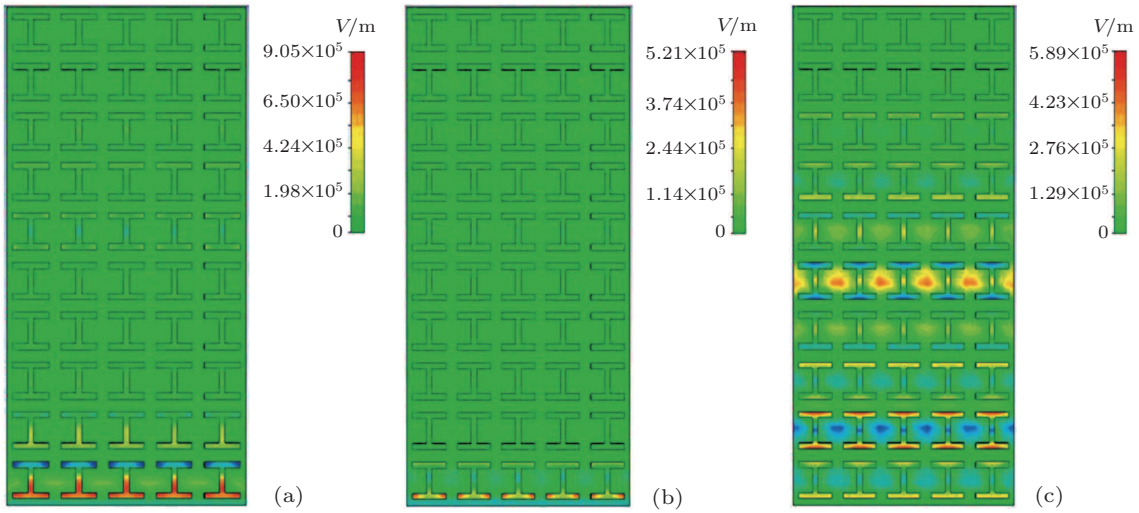


Fig. 6. (color online) Electric field distributions of the 3D plasmonic crystal with groove depth $H = 30$ μm and distance $L = 40$ μm at three typical frequencies: (a) 1.5 THz, (b) 2.0 THz, and (c) 2.9 THz.

Lastly, we want to have an intuitive understanding of the resonance of our 3D plasmonic crystal. Figure 6 shows the electric field distributions of the 3D plasmonic crystal with the groove depth $H = 30$ μm and the distance $L = 40$ μm at three typical frequencies (1.5 THz, 2.0 THz, and 2.9 THz, respectively). From Fig. 6, it can be seen that the transmission of THz waves is close to zero in the off-state, and the modulation depths are all over 40 dB according to the detailed spectral data. Although 1.5 THz, 2 THz, and 2.9 THz are all within resonance frequency range, the electric field distributions and the resonance modes are different, so several resonant modes for surface plasmon resonance exist in this system. It is precisely because the double-layer 3D plasmonic crystal structure can provide more resonant modes that the resonant bandwidth can be greatly broadened.

4. Conclusion

In summary, the transmission and filtering properties of the 3D plasmonic crystal have been investigated in the THz regime. We find that, for our design, both the passband and the bandgap are ultra-wide, and their transmittances are very close to 1 and 0, respectively. Furthermore, the transition between the passband and the bandgap is very rapid. Therefore, our design's filtering characteristics are far superior to those of the traditional single-layer structure. The resonant frequency blueshifts gradually from 0.88 THz to 1.30 THz as the distance L increases. As a result, we can dynamically control the bandwidths of the bandgap and passband. In addition, for an intuitive understanding of the resonance, the dispersion relations of these modes and electric field distributions are presented to analyze the mechanisms generating the bandgaps and frequency shifts. Our design and work can be applied to a tunable THz filter and switch, and it also has significant reference value for the design of other THz functional devices.

References

[1] Chan W L, Moravec M L, Baraniuk R G and Mittleman D M 2008 *Opt. Lett.* **33** 974
[2] Wu L, Ling F R, Liu T, Liu J S, Xu Y B and Yao J Q 2011 *Opt. Express* **19** 5118
[3] Xu J Z, Yuan T, Samuel M and Zhang X C 2003 *Chin. Phys. Lett.* **20** 1266
[4] Brucherseifer M, Nagel M, Bolivar P H, Kurz H, Bosserhoff A and Büttner R 2000 *Appl. Phy. Lett.* **77** 4049
[5] Maier S A, Andrews S R, Martín-Moreno L and García-Vidal F J 2006 *Phys. Rev. Lett.* **97** 176805
[6] Seo M A, Park H R, Koo S M, Park D J, Kang J H, Suwal O K, Choi S S, Planken P C M, Park G S, Park N K, Park Q H and Kim D S 2009 *Nat. Photonics* **3** 152

[7] Park D J, Choi S B, Ahn Y H, Rotermund F, Sohn I B, Kang C, Jeong M S and Kim D S 2009 *Opt. Express* **17** 12493
[8] Lee J, Lee K, Park H, Kang G, Yu D H and Kim K 2010 *Opt. Lett.* **35** 2254
[9] Chen Z and Zhang Y X 2013 *Chin. Phys. B* **22** 067802
[10] Pendry J B, Holden A J, Robbins D J and Stewart W J 1999 *IEEE Trans. Microwave Theory Tech.* **47** 2075
[11] Shelby R A, Smith D R and Schultz S 2001 *Science* **292** 77
[12] Pendry J B 2000 *Phys. Rev. Lett.* **85** 3966
[13] Liu Z W, Lee H, Xiong Y, Sun C and Zhang X 2007 *Science* **315** 1686
[14] Bingham A, Zhao Y and Grischkowsky D 2005 *Appl. Phys. Lett.* **87** 051101
[15] Dai X Y, Xiang Y J, Wen S C and He H Y 2011 *J. Appl. Phys.* **109** 053104
[16] Xue W R, Guo Y N and Zhang W M 2010 *Chin. Phys. B* **19** 017302
[17] Lee E S, So J K, Park G S, Kim D, Kee C S and Jeon T I 2012 *Opt. Express* **20** 6116
[18] Fan F, Li W, Gu W H, Wang X H and Chang S J 2013 *Photonics Nanostruct.* **11** 48
[19] Ye L F, Xu R M, Zhang Y and Lin W G 2011 *Chin. Phys. Lett.* **28** 124102
[20] Dionne J A, Sweatlock L A, Atwater H A and Polman A 2006 *Phys. Rev. B* **73** 035407
[21] Lin X S and Huang X G 2008 *Opt. Lett.* **33** 2874
[22] Li G H, Chen X S, Li O P, Shao C X, Jiang Y, Huang L J, Ni B, Hu W D and Lu W 2012 *J. Phys. D: Appl. Phys.* **45** 205102
[23] Neutens P, Lagae L, Borghs G and van Dorpe P 2012 *Opt. Express* **20** 3408
[24] Hosseini A and Massoud Y 2006 *Opt. Express* **14** 11318
[25] Li G H, Chen X S, Ni B, Li O P, Huang L J, Jiang Y, Hu W D and Lu W 2013 *Nanotechnology* **24** 205702
[26] Ulbricht R, Hendry E, Shan J, Heinz T F and Bonn M 2011 *Rev. Mod. Phys.* **83** 543
[27] Raether H 1988 *Surface Plasmons on Smooth and Rough Surfaces and on Gratings* (Berlin: Springer-Verlag) p. 1
[28] Hibbins A P, Sambles J R and Lawrence C R 2002 *Appl. Phys. Lett.* **80** 2410
[29] Sobnack M B, Tan W C, Wanstall N P, Preist T W and Sambles J R 1998 *Phys. Rev. Lett.* **80** 5667
[30] Kats M A, Woolf D, Blanchard R, Yu N F and Capasso F 2011 *Opt. Express* **19** 14860